Soft Matter

ROYAL SOCIETY
OF CHEMISTRY

COMMUNICATION
Mingfeng Wei, Lixin Wu *et al.*
Cluster-directed ionic framework supramolecular hydrogel
with high-temperature tolerability and enhanced water
evaporation

20 YEARS
ANNIVERSARY

Check for updates

Cluster-directed ionic framework supramolecular hydrogel with high-temperature tolerability and enhanced water evaporation†

Jiaxu Wang, Liang Yue, Mingfeng Wei,* Bao Li [ID] and Lixin Wu [ID] *

Supramolecular hydrogels have been constructed with flexible 2D ionic framework assemblies comprised of a stick-shaped di-cationic pseudo-rotaxane and polyanionic nanoclusters through electrostatic interactions. This type of small-molecule hydrogel exhibits excellent thermal stability at high temperature and shows an efficient reduction of water evaporation enthalpy.

Hydrogels constitute a kind of emerging soft matter that, by forming a crosslinked assembly of gelators, can fix huge amounts of water molecules, and hence show diverse potential applications.[1,2] Besides the interest in the inherent structural and mechanical characteristics of hydrogels, there is also great interest in finding more applications for them, for example in flexible electronic devices, protection layers for electrodes, medical coatings and anti-bacterial materials.[3,4] These network structures have been demonstrated to be efficient materials for promoting water evaporation and are expected to find applications in seawater desalination, sewage treatment, agriculture, and energy.[5,6] As a result, developing extended physicochemical features like wide range of or higher gel transition temperatures for these purposes have become highly desired. Typically, hydrogels that can maintain the gel state at temperatures higher than the boiling point of water can show or lead to many important phenomena and have practical values.[7,8] For example, hydrogels have been used for desalination of sea water *via* rapid evaporation of accommodated water, and the gel structures that can withstand a wider range of temperatures are favourable for this process.[9,10] To meet the above needs, those polymers forming a more stabilized gel structure than do small-molecule gelators are often used.[11,12] However, finding the right balance between stabilizing the gel structure and incorporating additional functionalities must be considered, and the introduction of extra components

has been a common approach. With this route, blocking phase separation of components of the gel at high temperature still needs to be achieved. Therefore, finding novel gelators displaying both gel stability and additional functions represents a new path to face the challenges in this field.

Molecular framework structures with high specific surface areas and tuneable physicochemical properties have been applied to various aspects of chemistry and material science.[13,14] However, the synthetic frameworks are all prepared as powdered solids, which plagues the extension of the uniform porosity into soft materials.[15,16] As a result, increasing processability by creating structural flexibility becomes important.[17,18] The current hydrogels bearing the powdered frameworks are prepared by considering polymer composition.[19,20] The inherent drawback of this approach is that the content and structural inhomogeneity need to be controlled deliberately. Therefore, developing a direct construction of hydrogels by using the framework itself as a gelator remains critical. Fortunately, the supramolecular frameworks constructed *via* intermolecular interactions facilitate the regulation of water molecules within the framework and offer a possible pathway for achieving both an increased gel transformation temperature and increased evaporation efficency.[21–23]

Polyoxometalates (POMs) are discrete metal–oxide clusters with well-defined chemical compositions and structures. Their diverse architectures, uniform morphologies, and multiple negative charges make them strong candidates for ionic self-assembly.[24–26] The geometric properties of POMs, along with the non-saturated binding modes and non-preferential direction of ionic interactions, steric effects, and charge-neutralization–induced hydrophobic effects highlight the exceptional characteristics of POM-based ionic self-assemblies.[27,28] In this context, we chose POM clusters with three negative charges to co-assemble with cationic pseudo-rotaxane bromide (CPR·2Br) comprised of di-α-cyclodextrin (CD)-shielded di-cationic guest bromide (BCG·2Br) for the construction of an ionic supramolecular framework (ISF) hydrogel. Due to the limited area around the surface of the clusters, the dynamic crosslinking of multiple non-covalent

State Key Laboratory of Supramolecular Structure and Materials, College of Chemistry, Jilin University, Changchun 130012, P. R. China.
E-mail: weimf19@mails.jlu.edu.cn, wulx@jlu.edu.cn
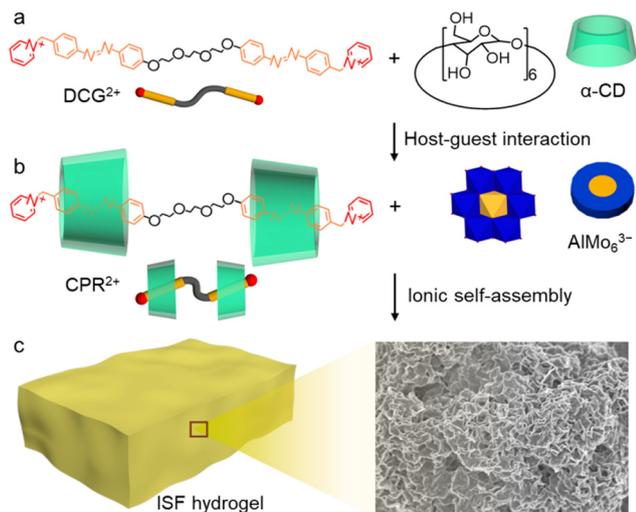
Scheme 1 Schematic chemical structures and representations of (a) the building blocks of the developed hydrogel, namely di-cationic guest DCG·2Br and host molecule α-CD, (b) pseudo-rotaxane component (CPR·2Br) and POM cluster $AlMo_6^{3-}$, and (c) formation of ISF hydrogel via ionic self-assembly, with its SEM image also shown.
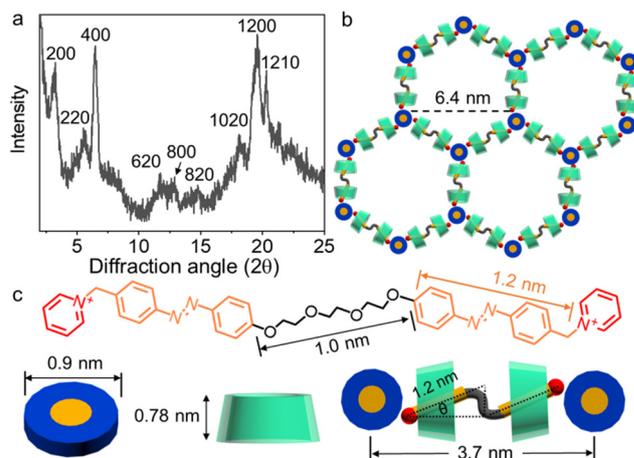

Fig. 1 (a) XRD pattern of the ISF xerogel, (b) corresponding simulated structure showing side spacing in ab plane, and (c) analysis of the framework structure in reference to the sizes of the $AlMo_6^{3-}$ and CPR^{2+} components.

interactions drives an angle-specific connection of CPR^{2+} with POMs, leading to two-dimensional adaptive frameworks. Depending on the combined hydrophilicity of the POMs, CD host and cationic guest, the self-assembled framework structure can rapidly form a hydrogel (Scheme 1) with strong thermal stability and a high gel transition temperature, specifically one exceeding 110 °C. The ISF hydrogels that integrate the properties of the gel and hierarchical porous channels considerably enhance water transport without gel structure collapse occurring at increased temperature. The ionic interactions and hydrophilicity of the used components support the association of water with the framework assembly while the ionic binding prevents much dissociation from occurring when the temperature of the environment changes, albeit with a reduced water evaporation enthalpy. The replacement of POMs with species containing different charges can further optimize the ionic framework hydrogels and yield diverse applications.

CPR·2Br and a typical POM, namely the sodium salt of $Na_3[AlMo_6O_{24}]$ ($AlMo_6^{3-}$) (Scheme 1a and b), were prepared following the previous procedures.[29,30] Upon the addition of the disk-shaped $AlMo_6^{3-}$ cluster solution into the CPR^{2+} solution with an equivalent charge ratio, a precipitate emerges as the cationic heads at both ends of CPR^{2+} cap the polyanionic cluster with electrostatic interactions (Scheme 1c). The detected binding proportion is in good agreement with the 3:2 stoichiometric molar ratio, indicative of complete charge neutralization (Table S1, ESI†). Considering chemical composition, CPR^{2+} adopts a rigid stick-shaped conformation in the assembly. Thus, it is inferred that the formed ionic assembly is derived from a [2+3] type connection. Due to the charges of $AlMo_6^{3-}$ locating at the edge of disk architecture with a diameter of 0.9 nm, the heads of CPR^{2+}s surround the cluster at an equal distance from each other. Although the guest molecule itself can form a gel in

water, the gel transforms into a sol when host CD is added, because of the increased hydrophilicity and the weakened intermolecular interactions between CPR^{2+}s. Upon adding $AlMo_6^{3-}$ to this solution, a hydrogel emerges again. Such a gelation is apparently driven by the co-assembly of the cluster via electrostatic interactions and subsequent crosslinking of assemblies (Fig. S1, ESI†). The critical gelation concentration (CGC) was measured to be less than 4.5 wt% by adjusting the total solute concentration, while keeping composition ratio of each component of the hydrogel (Fig. S2, ESI†).

The X-ray diffraction (XRD) measurements taken reveal the assembly structure of the hydrogel at a concentration of 9.4 wt%. A two-dimensional (2D) framework structure with a distinct hexagonal packing form can be concluded from these data. A series of diffraction peaks observed at 3.2, 5.5, 6.4, 11.7, 12.8, 14.7, 18.1, and 19.6° can be attributed to the (200), (220), (400), (620), (800), (820), (1020), and (1200) planes (Fig. 1a). The hexagonal lattice parameter a gives a pore diameter of 6.4 nm and a length of 3.7 nm for each side of the hexagonal packing assembly (Fig. 1b). Based on the calculated lengths of the rigid group and flexible feature of the EO chain at a fully contracted state with the guest cations, the XRD data match well with the sizes of $AlMo_6^{3-}$ and CPR^{2+} in the ISF structure (Fig. 1c). Because of the lack of any crystalline plane at the c-axis according to the diffraction pattern, a single layer of the 2D framework can be interpreted.[31] Meanwhile, the order of the ISF assembly structure gradually increases upon the change from sol to gel with the increase of the concentration (Fig. S3, ESI†). The freeze-dried hydrogel's SEM images display a large-scale, cross-plied laminate structure that confines water within its pores (Fig. S4, ESI†). Further observation using transmission electron microscopy (TEM) reveals the existence of distinct sheet-like structures with dimensions of about 2 μm. The magnified image points out the even dispersion of the clusters within the hydrogel assemblies (Fig. S5, ESI†). Thus, it can be deduced that the flexible 2D single layer ISF as a nanosized assembly accommodates water molecules to form the observed hydrogel.

Rheological analysis of the hydrogel indicates its mechanical properties. Due to the weak connections of the supramolecular framework assemblies with each other, the modulus of the hydrogel is not high (storage moduli, $G' \leq 10\ G''$, loss moduli) (Fig. 2a).[32] Based on the strain at the crossover of G' and G'', the ISF hydrogel is concluded to be quite rigid (Fig. 2b). Compared with the mechanical properties of guest cations and CPR·2Br aqueous solution, the strength of hydrogel after adding $AlMo_6^{3-}$ is significantly improved (Fig. S6, ESI†). Interestingly, the hydrogel exhibits excellent thermal stability, better than those of general supramolecular gels comprised of small molecules. Characterization of the gel-to-sol transition using the inversion method indicates the lack of any such transition when the hydrogel is heated to 130 °C, except for the cracking of the gel. Meanwhile, testing the effect of temperature on the stability of the gel shows the hydrogel framework maintaining its gel features at 120 °C. (Fig. 2c and Fig. S7, ESI†). The greatly increased gel stability can be ascribed to the crosslinking of POM clusters in the porous network structure, which is almost unaffected by changes in the temperature in the tested temperature range. The lack of any considerable effect of temperature may be due to the use of ionic interactions rather than the hydrophobic force and simple packing of small molecular units. Additionally, the multiple hydrogen bonds between cyclodextrins of adjacent framework layers help maintain the initial gel assembly during heating. The XRD analysis of the hydrogel dried under different temperature conditions demonstrates that the diffraction peaks attributed to the ordered framework structure remain almost unchanged upon heating to 80 °C and, upon heating to 120 °C, show only a slight decrease in intensity, along with a slight shift in the diffraction angle, indicating minor shrinkage of the framework's side lengths (Fig. S8, ESI†). Correspondingly, the observations of the morphology of the hydrogel under these temperature conditions indicate that the crosslinked nanosheet assemblies are maintained after drying the hydrogel at 80 °C and 100 °C (Fig. S9 and S10, ESI†). The ISF nanosheet assemblies start to merge and finally transform into the highly combined assemblies at 120 °C (Fig. S11, ESI†).

Even at this stage, the gel structure is not broken into the disconnected sol. Therefore, the lack of any apparent gel–sol transition can be deduced to be due a rapid evaporation of water rather than the disassembly triggering a collapse of the gel when the temperature exceeds the boiling point of water.

To demonstrate the influence of the charge numbers, we prepared a series of POMs having similar diameters but a spherical shape with different negative charges for the construction of hydrogels with CPR^{2+}. Under the condition of equivalent charge ratio, the gel transition temperature gradually decreases with increasing charge number (Table S2, ESI†). For the $PW_{11}VO_{40}$ cluster (PWV^{4-}), typically the hydrogel completely collapses when heated to 78 °C and recovers its hydrogel form about 2 h after being cooled back down to room temperature, indicative of good reversibility (Fig. S12, ESI†). Under the condition of POM and CPR^{2+} 1:1 charge ratio, with the same CPR^{2+} proportion, the more negative charges of POM would reduce the number of the cluster and, therefore, the binding positions, directly resulting in a decrease of hydrogel thermal stability. In other words, the reduced cluster content decreases the concentration of gelator, which also causes the gel transition temperature to decrease with increasing charge number of POM in reference to $AlMo_6^{3-}$. As the final number of CPR^{2+} species surrounding POMs can be modulated by controlling the molar ratio between them, we can increase the content of POMs to increase the quantity of ionic crosslinking nodes and hence enhance the thermostability. For example, upon adding $[CoW_{12}O_{40}]^{6-}$ (CoW^{6-}) while keeping its molar ratio of 2:3 with CPR^{2+}, the gel–sol transition temperature increases from 76 °C to 96 °C. The lower transition temperature than that of $AlMo_6^{3-}$ can be explained as the excess charges of CoW^{6-} in the framework assembly yielding a negatively charged surface, which causes both enhanced hydrophilicity and electrostatic repulsion. The experimental results indicate that a larger excess of charges of POMs leads to the lower gel–sol transition temperature (Table S3 ESI†). Besides charge numbers, the size of the used clusters affects the tolerance of the framework hydrogels to heating. d Simple polyanions of phosphate PO_4^{3-} form an assembly with CPR^{2+} via charge compensation. However, the gel–sol transition temperature of this assembly is only about 62 °C, much lower than those of the hydrogels constructed using POMs (Fig. S13, ESI†). This difference is due to the electrostatic interactions formed by the simple anion being weaker than those formed by POMs. The stereospecific blockade of CD at the head position during the formation of the framework assembly may also cause the ionic interactions to easily break at increased temperature.

The hydrogel structure integrates the hierarchical channels including micropores among ISF assemblies and nanopores in inner frameworks. While the micropore allows for effective water transport, the hydrogel assembly displays a larger area exposed to the external environment for interaction with water. This property helps to reduce the evaporation enthalpy of the water and promotes the formation of water vapor by weakening the hydrogen bonding between water molecules.[33] A DSC measurement of the water evaporation enthalpy shows pure water having an evaporation enthalpy of 2158 J g^{-1} and a
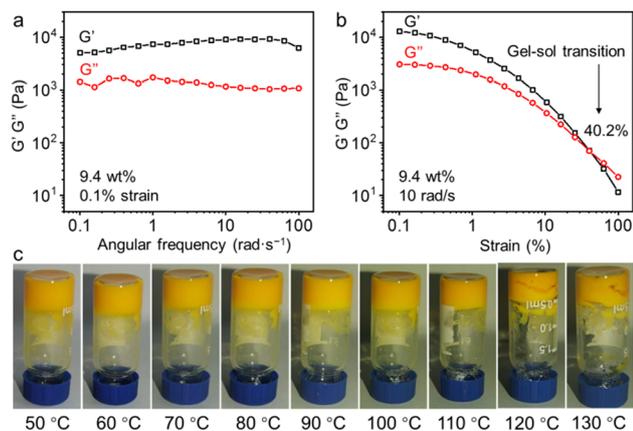

Fig. 2 (a) Plots showing the rheology of the prepared ISF hydrogel as a function of angular frequency, (b) strain analysis of the hydrogel, and (c) photographs showing the hydrogel stability from 50 °C to 130 °C.
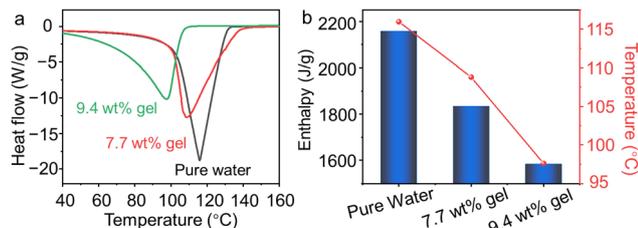
Fig. 3 (a) Plots of heat flow *versus* temperature for pure water and ISF hydrogels (7.7 wt% and 9.4 wt%), and (b) evaporation enthalpies of pure water and ISF hydrogels (7.7 wt% and 9.4 wt%).

critical temperature of 116.0 °C (Fig. 3a) with robust electric conductivity.[34] Upon adding either of a couple of different mass fractions of hydrogel, a noticeable reduction of the evaporation enthalpy occurs due to the increased surface area of the framework assembly. Correspondingly, upon increasing the hydrogel mass fraction, the evaporation enthalpy decreases from 1833 J g^{-1} to 1583 J g^{-1}, and the critical temperature from 108.8 °C to 97.6 °C (Fig. 3b), due to rapid evaporation. The total evaporation enthalpy decreases by 26.6% and the critical temperature decreases by 15.8%, indicating that the presence of the ISF hydrogel structure greatly reduces the energy for evaporation of water, thereby facilitating the formation of water vapor.[35] The evaporation experiment shows that at 80 °C, the presence of the hydrogel increases the mass of evaporated water by ∼10% relative to the control (Fig. S14, ESI†).

Conclusions

2D ISF assemblies with uniform pore structures have been constructed into hydrogel soft materials stabilized by electrostatic interactions made between cationic pseudo rotaxane and inorganic clusters, without the support of any additive components. This hydrogel, bearing a flexible crosslinked network structure, exhibits high thermal stability, even at temperatures much higher than the boiling point of water. This property allows the hydrogel to withstand a wide temperature range, including high-temperature water evaporation. The preliminary characterization done shows that the hierarchical porous channels are favourable for water transport, thereby reducing the water evaporation enthalpy. These results provide a strong potential for further functionalization of ion-organic frameworks in high-performance supramolecular hydrogels.

Data availability

The data that support the findings of this study are available from the corresponding author upon reasonable request.

Conflicts of interest

There are no conflicts to declare.

Notes and references

1 S. Bianco, M. Hasan, A. Ahmad, S.-J. Richards, B. Dietrich, M. Wallace, Q. Tang, A. J. Smith, M. I. Gibson and D. J. Adams, *Nature*, 2024, **631**, 544–548.

2 Y. Yuan, Q. Q. Zhang, S. M. Lin and J. L. Li, *Prog. Mater. Sci.*, 2025, **148**, 101378.

3 L. Zhang, C. Y. Zhang, J. Min, C. L. Liu, S. Z. Mao, L. Y. Wang, B. Yang and Z. Y. Dong, *Chem. Res. Chin. Univ.*, 2023, **39**, 736–740.

4 S. X. Lan, Y. Y. Mao, B. P. Zhou and W. B. Hu, *Nano Energy*, 2025, **134**, 110572.

5 R. X. Bai, X. Yang, J. Zhao, Z. M. Zhang and X. Z. Yan, *Chem. Res. Chin. Univ.*, 2023, **39**, 777–781.

6 C. X. Shao and L. T. Qu, *Acta Phys. – Chim. Sin.*, 2023, **39**, 2306004.

7 V. Kumaravel, J. Bartlett and S. C. Pillai, *Adv. Energy Mater.*, 2021, **11**, 2002869.

8 T. Li, Y. Luo, S. H. Wu, X. Xia, H. Zhao, X. Xu and X. B. Luo, *ACS Appl. Mater. Interfaces*, 2023, **15**, 29854–29865.

9 X. Y. Jing, F. F. Liu, T. Abdiryim and X. Liu, *Chem. Eng. J.*, 2024, **479**, 147519.

10 H. Q. Zou, X. T. Meng, X. Zhao and J. S. Qiu, *Adv. Mater.*, 2023, **35**, 2207262.

11 X. Y. Zhou, Y. H. Guo, F. Zhao, W. Shi and G. H. Yu, *Adv. Mater.*, 2020, **32**, 2007012.

12 X.-T. Yang, H. Lin, J.-C. Zhang, G. Q. Yu, Y. L. Peng and Q.-F. An, *Chem. Eng. J.*, 2024, **479**, 147868.

13 J. Lü and R. Cao, *Angew. Chem., Int. Ed.*, 2016, **55**, 9474–9480.

14 L. P. Skala, C. L. Stern, L. Bancroft, C. M. Moisanu, C. Pelkowski, X. Aguilar-Enriquez, J. L. Swartz, M. R. Wasielewski and W. R. Dichtel, *Chemistry*, 2023, **9**, 1208–1220.

15 Z. X. Sun, R. Wang and I. V. Kozhevnikov, *Coord. Chem. Rev.*, 2025, **524**, 216304.

16 Y. Zhang, B. Li and L. X. Wu, *Acta Phys. – Chim. Sin.*, 2024, **40**, 2305038.

17 X. Y. Mao, X. Q. Ding, Q. Wang, X. P. Sun, L. Qin, F. Huang, L. H. Wen and X. W. Xiang, *Small*, 2024, **20**, 2308739.

18 S. P. Jia, Y. J. Liu, L. Q. Hao, J. Y. Ni, Y. J. Wang, Y. Yang, Y. Chen, P. Cheng, L. Chen and Z. J. Zhang, *J. Am. Chem. Soc.*, 2023, **145**, 26266–26278.

19 Y. L. Wang, H. Peng, H. M. Wang, M. C. Zhang, W. Zhao and Y. Y. Zhang, *Chem. Eng. J.*, 2022, **450**, 138216.

20 C. X. Li, S. J. Cao, J. N. Lutzki, J. Yang, T. Konegger, F. Kleitz and A. Thomas, *J. Am. Chem. Soc.*, 2022, **144**, 3083–3090.

21 Z.-T. Li, S.-B. Yu, Y. M. Liu, J. Tian and D.-W. Zhang, *Acc. Chem. Res.*, 2022, **55**, 2316–2325.

22 M. Wei, B. Li and L. Wu, *Adv. Sci.*, 2023, **10**, 2207047.

23 M. Wei, F. Duan, B. Li, Y. Wang and L. Wu, *Nano Lett.*, 2024, **24**, 4124–4131.

24 Q. D. Liu, Z. Sheng, W. X. Shi, X. J. Cheng, X. X. Xu and X. Wang, *J. Am. Chem. Soc.*, 2024, **146**, 12819–12827.

25 Z. B. Zheng, P. Y. Yu, R. Wang, J. Y. Tan, J. Zhang and X. H. Wan, *Chem. Commun.*, 2023, **59**, 191–194.

26 Z. X. Zhu, G. H. Zhang, B. Li, M. H. Liu and L. X. Wu, *Nat. Commun.*, 2024, **15**, 8033.

27 S. C. Chai, F. R. Xu, R. C. Zhang, X. L. Wang, L. Zhai, X. Li, H.-J. Qian, L. X. Wu and H. L. Li, *J. Am. Chem. Soc.*, 2021, **143**, 21433–21442.

28 T. Buchecker, P. Schmid, I. Grillo, S. Prévost, M. Drechsler, O. Diat, A. Pfitzner and P. Bauduin, *J. Am. Chem. Soc.*, 2019, **141**, 6890–6899.

29 C. Y. Yin, F. R. Jiang, B. Li and L. X. Wu, *Soft Matter*, 2019, **15**, 5034–5041.

30 H. Ai, Y. Wang, B. Li and L. X. Wu, *Eur. J. Inorg. Chem.*, 2014, 2766–2772.

31 L. Yue, S. Wang, D. Zhou, H. Zhang, B. Li and L. X. Wu, *Nat. Commun.*, 2016, **7**, 10742.

32 M. Li, H. Zhu, S. Adorinni, W. Xue, A. Heard, A. M. Garcia, S. Kralj, J. R. Nitschke and S. Marchesan, *Angew. Chem., Int. Ed.*, 2024, **63**, e202406909.

33 J. J. Koh, G. J. H. Lim, S. Chakraborty, Y. X. Zhang, S. Q. Liu, X. W. Zhang, S. C. Tan, Z. Y. Lyu, J. Ding and C. B. He, *Nano Energy*, 2021, **79**, 105436.

34 X. Zhou, Y. Guo, F. Zhao and G. Yu, *Acc. Chem. Res.*, 2019, **52**, 3244–3253.

35 X. Y. Hu, P. Y. Hu, L. Liu, L. M. Zhao, S. Y. Dou, W. B. Lv, Y. Long, J. Wang and Q. W. Li, *Matter*, 2024, **7**, 1–12.